Design and AC Modeling of a Bipolar GNR-h-BN RTD With Enhanced Tunneling Properties and High Robustness to Edge Defects

Mahdi Khoshbaten and Seyed Ebrahim Hosseini

***Abstract*— This paper proposes a robust to defects and short length device (RDSLD), a newly in-plane resonant tunneling diode (RTD), and its ac-modeling with the minimum length of 3 nm. The proposed structure has robust performance in the presence of defects. It also has a high degree of flexibility in tuning electronic specifications. By using bipolar doping and a special h-boron nitride barrier pattern, these unique features are obtained. The simulation results verify that the proposed structure has the potential for replacing conventional RTD diodes. Such that the peak-to-valley ratio (PVR) and the maximum current of 4500, 450 nA for perfect bowtie and 3.45, 1256 nA for rhombic barrier shape structure are obtained, respectively. Also, negative differential resistance (NDR) is observed in all of the structures with vacancy and impurity defects. The effect of the geometrical parameters on the charge transmission of the device is another issue that is addressed in this paper. Furthermore, the analytical and numerical capacitance model parameters are presented.**

***Index Terms*— Circuit modeling, bipolar doping, boron nitride (BN), graphene, resonant tunneling diodes (RTDs), robust to defects.**

I. Introduction

THE negative differential resistance (NDR) effect in the current–voltage characteristics of resonant tunneling diode (RTD) devices makes it possible for us to use them in a variety of applications, including oscillators, amplifiers, multi logic gates, and switching circuits [1]–[3]. Within the next few years, fundamental physical limits will restrict the downscaling of integrated circuits. Thus, researchers are looking for alternative materials based on the semiconductor technology roadmap [4]. Meanwhile, graphene has attracted the attention of many researchers due to its popular electronic and mechanical properties [5]–[9]. On the other hand, it suffers from extreme sensitivity to defects [10], lack of a bandgap [11], band structure variations versus geometric changes, and strong interaction with the substrate [12].

Manuscript received May 7, 2019; revised June 13, 2019; accepted June 18, 2019. Date of publication July 8, 2019; date of current version July 23, 2019. The review of this paper was arranged by Editor P. J. Fay. *(Corresponding author: Seyed Ebrahim Hosseini.)*

The authors are with the Electrical Engineering Department, Ferdowsi University of Mashhad, Mashhad 9177948974, Iran (e-mail: m.khoshabten@mail.um.ac.ir; ehosseini@um.ac.ir).

Color versions of one or more of the figures in this paper are available online at http://ieeexplore.ieee.org.

Digital Object Identifier 10.1109/TED.2019.2924451

Several works have been done on graphene RTDs as reported in the literature. In [13], different structures of modulated armchair graphene nano-ribbon (AGNR)-RTDs are constructed by introducing hexagonal antidotes, hexagonal boron nitride (BN) doping atoms and their combination in the middle of pristine AGNRs. A new platform of AGNR-based RTD using the effects of the strain is one of the other studies [14]. In [15], step-like zigzag graphene nanoribbons (ZGNRs) with different step widths are designed. The device performance of graphene nanoribbons (GNRs) RTDs with different shapes and dimensions has been addressed in [16]–[19].

In all of the above mentioned and similar studies [1], [20]–[25], the maximum current value in microamperes multiplied by peak-to-valley ratio (PVR) which is referred to as Current-PVR product (CP) is usually much less than unity. This property states that there is always a tradeoff between PVR and maximum current value, and a balance between them should be somehow established. For the first time in this paper, CP values greater than one are achieved in all of the proposed platforms. Furthermore, the proposed structures that are referred to as robust to defects and short length device (RDSLD) have superior features such as: 1) robustness to edge and vacancy defects and adsorbed impurity; 2) fixed bias position of maximum current; 3) great PVR and CP values; 4) high current density; 5) low-power dissipation; and 6) stable operation for the device length range of about 3 to 20 nm.

It should be mentioned that nanometer-scale GNR synthesis and direct merging of graphene and h-BN into in-plane graphene/h-BN hybrids with well-controlled shape and size of doping domains have been experimentally realized by [26]–[35].

This paper is organized as follows: In Section II, the four proposed structures are described in detail. In Section III, the parameters of the ac equivalent circuit are determined. In Section IV, the results of I–V curve simulations and the effects of defects and geometrical parameters on the performance of the devices are presented. Conclusions are finally drawn in Section V.

II. Proposed Devices

Fig. 1 shows the four proposed structures for RTDs. All of the structures consist of a thin barrier and two positive and negative heavily doped (n-two [36] and p-two pole) regions

0018-9383 © 2019 IEEE. Personal use is permitted, but republication/redistribution requires IEEE permission.
See http://www.ieee.org/publications_standards/publications/rights/index.html for more information.

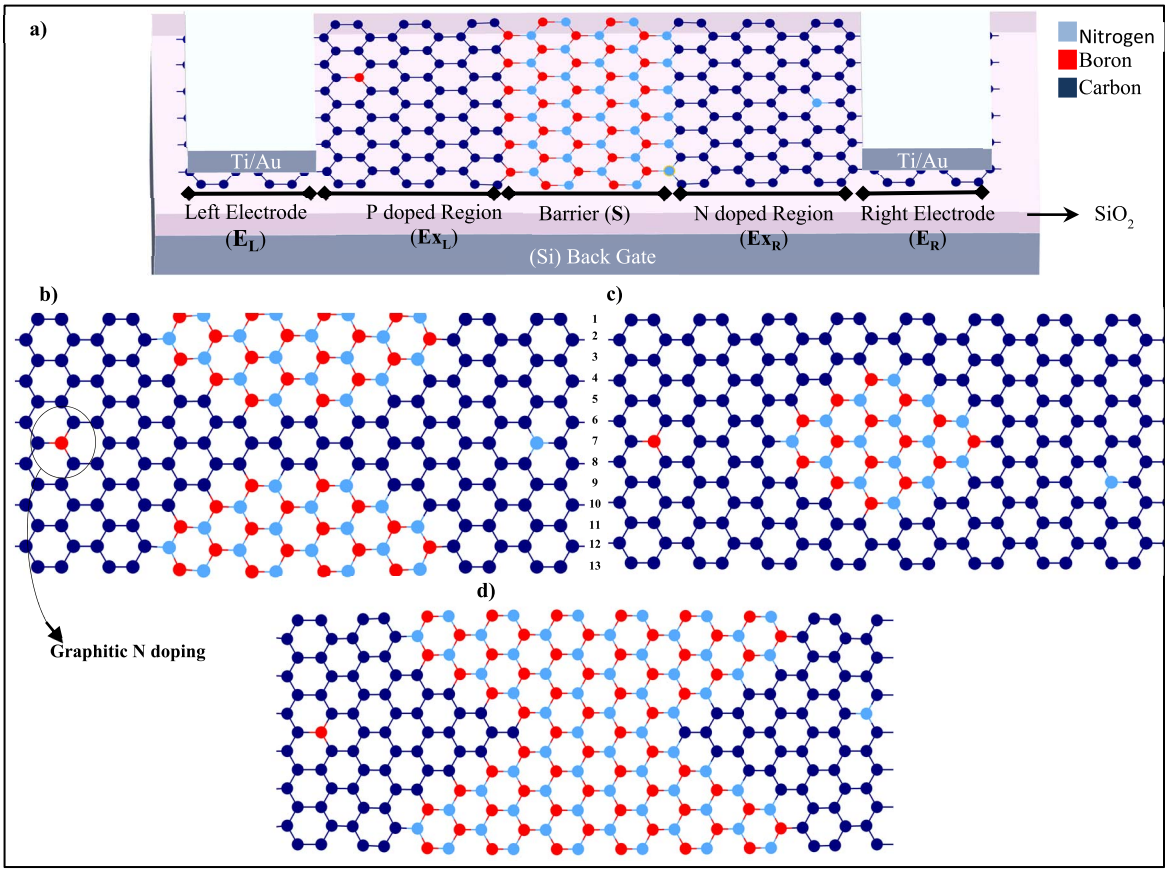

Fig. 1. Proposed basic structures with (a) flat, (b) imperfect bowtie, (c) rhombic, and (d) perfect bowtie barrier. Substrate and electrode regions (that are shown in a) are eliminated for simplicity. The impurity density is about 4×10^{17} cm^{-2}. "Index" definition is denoted with numbers on the right side of b.

of the same length. Device names are chosen based on their barrier shapes. It should be noted that all of the proposed structures have SiO_2 substrates and Ti/Au electrodes [Fig. 1(a)], which are not included in the figures for the sake of simplicity. Moreover, the dangling bonds of graphene are passivated by hydrogen or BN [27], which are ignored in this research study in order to avoid unnecessary complexity.

The graphene layer can be synthesized such that the substrate does not have a significant influence on the electronic properties of the device. It can be achieved using embedded h-BN trenches [27], quasi-free-standing graphene [37] or transfer of graphene after synthesis.

Significantly reducing the dimensionality in n+ p+ junction expands the depletion width [38]. Thus, a thin barrier (h-BN) is required, along with two-pole regions, to represent the NDR effect. This platform reduces the length of the structure to at least 3 and 1.2 nm in the normal direction. Bipolar doping also plays a crucial role in reducing the structure's sensitivity to defects, as discussed in more detail in the next section.

On the other hand, the bandgap of Graphitic n- and p-doped 10-GNR are calculated with values of 0.81 and 0.8 eV with 10^{17} cm^{-2} doping density, respectively. The results are in agreement with the previous studies [39]. Adding impurities causes three opposing effects: 1) improved charge tunneling because of the increased electron density; 2) reduced mobility (μ) due to the charged-impurity scattering [40]; and 3) causes graphene to act like a degenerate semiconductor as well as pseudo-metal material. Moreover, recent theoretical and experimental results have shown that charged impurities of graphene and its substrate have a vital role in the transport properties of graphene near the Dirac point [40]–[42]. Simultaneously, considering these parameters for a comprehensive survey of the proposed devices is essential.

Fig. 2 shows $|\Psi|^2$ or electron density in the proposed structures. Fig. 2 shows the availability of the energy states for charge transfer in all of the transport directions in both imperfect bowtie and rhombic barrier shaped structures. This difference, when compared with the previous studies, has led to an improvement in the maximum current value. In this regard, the barrier shape is the determinant parameter on the transmission of charges through the device.

Therefore, in the thinner GNRs, it is better to have a rhombic barrier shape to obtain high Ion current. In this situation, the edge energy states have a dominant contribution to the charge transport that results in charge transmission being more affected by the edge defects. In contrast, the thicker ones (widths greater than 20 nm) should have a Bowtie barrier shape to eliminate edge states and minimize I_{OFF} current.

From a different point of view, in the real space, doping atoms affect the charge pathway in such a way that it absorbs the charge to its spatial location. Atom-to-atom probability of charge transport (transmission pathway) which splits the

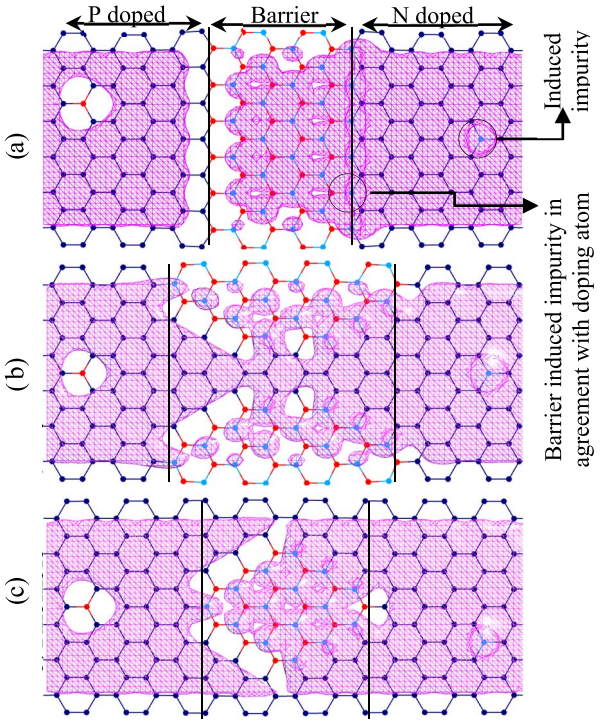

Fig. 2. Counter image of the intrinsic (without applied bias) spatial electron density of the proposed structures in hue-saturation-value color map with maximum density of 0.62×10^{15} cm^{-2}. Charged carrier transmission path and the effects of BN impurity are observable. (a) Flat. (b) Imperfect Bowtie. (c) Rhombic.

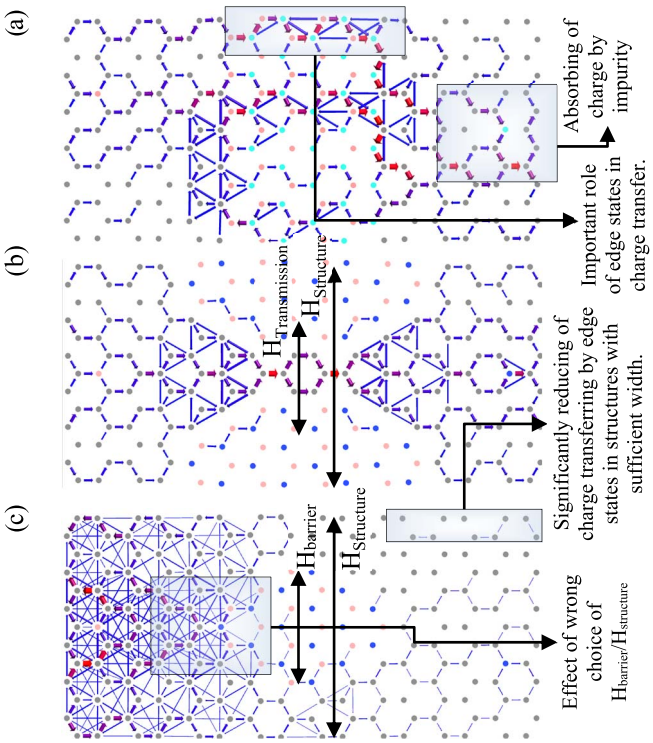

Fig. 3. Transmission pathways of the proposed structures that sum up to form the transmission coefficient. (a) Flat. (b) Imperfect Bowtie. (c) Rhombic.

transmission coefficient into local bond contributions (1) is shown in Fig. 3

$$T(E,V) = \sum_{m,n} T_{mn}(E,V) \tag{1}$$

where T_{mn} is the local transmission between all pairs of atoms m and n [43]. As shown in the right-hand side of the doped region of the flat barrier structure [Fig. 3(a)], impurities cause charge accumulation around them that we refer to as "Charge-Localization."

As the last point, in a rhombic (Imp. Bowtie) barrier shaped device, the constant value of $H_{\text{barrier}}/H_{\text{structure}}$ ($H_{\text{Transmission}}/H_{\text{structure}}$) should be less than 0.7 (0.3). Otherwise, the total transmission would degrade [Fig. 3(c)].

III. Device Current and Capacitance Modeling

In this paper, a semiquanum mode based on the analytical model is used. This model is developed based on T-FET operation mechanism. Considering the transverse "mode" (M) of the current transport and transmission coefficient (T) for the p+ n+ channel to conduct charge carriers through the device, conductance of the channel as defined based on the Landauer expression is as follows [44]:

$$G(E) = \frac{2q^2}{h} M(E) T^{\text{GNR}}_{\text{WKB-modified}}(E) \tag{2}$$

where

$$M(E) = W \frac{2|E|}{\pi(\hbar v_F)} \tag{3}$$

q and $v_F \approx 10^8 \cdot \text{cm} \cdot \text{s}^{-1}$ are the electron charge and the Fermi velocity, respectively. Also, h and $\hbar$ are the Planck and the reduced Planck fundamental constants, respectively. W represents the width of the GNR and the energy range for calculating transverse modes is denoted by $|E|$. The number of conducting channels at energy E is proportional to the width of the conductor. Considering the anode and cathode Fermi–Dirac statistics and the channel conductance expressed in Landauer formalism, the current can be calculated as follows:

$$I_d = \int dE\, G(E)\,(f_A(E) - f_K(E)). \tag{4}$$

The modified transmission probability is proposed based on [1], [45], [46] and the fact that the electron wave degrades exponentially in the barrier region versus the barrier thickness

$$T^{\text{GNR}}_{\text{WKB-modified}} = \alpha \exp\left(-\frac{\pi E_G^2}{4q\hbar v_F F}\right) \exp(-2\kappa) \tag{5}$$

where α is the normalization factor and E_G is the GNR bandgap. F is the electric field at the GNR-barrier junction and it is obtained from the trend proposed by Lu *et al.* [47]. The decay constant κ is related to the barrier material and its thickness (d_{barrier})

$$\kappa = \int_{d_{\text{barrier}}} dx \sqrt{2m^*_{\text{BN}}(U(x) - E)}/\hbar. \tag{6}$$

In the flat barrier structure, ($U(x)$–E) or the barrier height (Δb) is a constant value of 1.5 eV and the effective electron mass of (6) for h-BN is as follows, reported in [48]:

$$m^*_{\text{BN}} = \frac{E_{G,h-\text{BN}}}{2v_F^2} \approx \text{cons.} \tag{7}$$

Substituting the above equations along with the proposed modified transmission probability (5) in (4) results in an

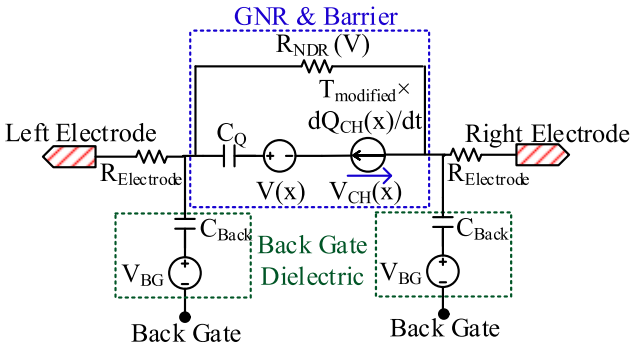

Fig. 4. Proposed modeling of the device capacitances.

expression for I_d (8). Finally, I_d is obtained (TH: Threshold) as follows [45], [46]:

$$I_d = \frac{\alpha(V_d)4q^3W}{\pi(\hbar^2 v_F)} \times \exp\left(-\frac{\pi E_G^2}{4q\hbar v_F F}\right) \times \exp(-\sqrt{2m^*\Delta b}/\hbar) \tag{8}$$

where $F = (E_{GNR} + qV_d - qV_{TH})/2\Lambda(\Lambda$ is p- and n-doped region widths [46]) and $\alpha(V_d) = -V_T(-V_{TH})\{\ln(1 + \exp((-V_{TH}/V_T))) - \ln(1 + \exp((V_{TH} - V_d/V_T))) - ((\pi V_T)^2/12)\}$

In (8), it is assumed that the thermionic contribution to current is negligible ($V_d >> KT/q(V_T)$). Moreover, V_{TH} is empirically fit to the values of 0.65, 0.6, and 0.8 V for flat, bowtie, and rhombic barrier shape structures, respectively [Fig. 8].

Fig. 4 is suggested here in order to obtain V_{CH} in (11) and then the device capacitance in order to validate the simulations that have been carried out. In Fig. 4, $V(x)$ is the voltage drop due to both anode-to-cathode bias voltage and substrate charge paddling. Moreover, C_Q is the quantum capacitance in the GNR. C_{Back} can be calculated as follows:

$$C_{Back}^{L/R} \approx \frac{\varepsilon A}{d} = \frac{\varepsilon_r \varepsilon_0 . L_{Ex}^{L/R}(N-1)(\sqrt{3})/2}{d_{Substrate}}. \tag{9}$$

In (9), L_{Ex} and N are the length of the doped region and structure index, respectively. In the SiO_2 substrate, ε_r is 3.9. Charge density and net charge are evaluated as follows [49]:

$$Q_{CH} \approx qW\frac{1}{E_{AV}}\int_0^{V_d}\left(\frac{\beta}{q}|V_{CH}|V_{CH} + n_{doping} + n_{Puddle}\right)dv$$

$$E_{AV} \approx \frac{1}{\left(\frac{(|Q_{net}| + qn_{puddle})\mu * W}{I_d} + \frac{\mu}{v_{SAT}}\right)} \tag{10}$$

where n_{puddle} is the residual charge density and Δ represents the spatial inhomogeneity of the electrostatic potential

$$n_{puddle} = \frac{\Delta^2}{\pi\hbar^2 v_F^2} \tag{11}$$

$$Q_{net}(x) \approx q\left(-\frac{q^2}{\pi(\hbar v_F)^2}|V_{CH}(x)|\,V_{CH}(x)\right)$$

$$v_{SAT} = \frac{\omega}{\sqrt{\pi\left(\frac{|Q_{net}(x)|}{q} + n_{puddle}\right)}}. \tag{12}$$

TABLE I
CAPACITANCE AND RESISTANCES OF THE FOUR PROPOSED STRUCTURES

Structure \ Property	R_{NDR}(KΩ)	C_Q(fF)
Flat Barrier	917	43.5
Imperfect Bowtie Barrier	240	19.54
Rhombic Barrier	112	6.23
Perfect Bowtie Barrier	420	32

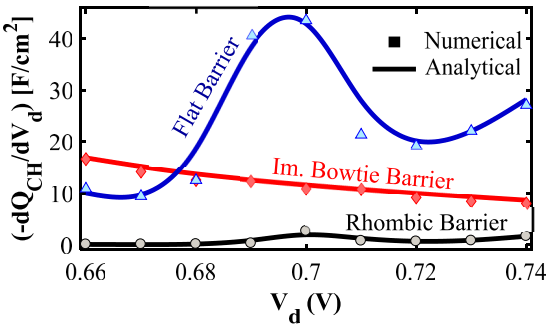

Fig. 5. C_Q capacitance versus V_d for different barrier shapes computed from numerical approach and analytical solution. We have assumed $\mu = 7000$ V·cm^{-2}·s^{-1}, $\Delta = 65$ meV, $\hbar\omega/2\pi = 56$ meV, $\varepsilon_r = 3.9$ and $N_d = 1 \times 10^{17}$cm^{-2}.

By applying Kirchhoff's law to the circuit shown in Fig. 4, an expression for V_{CH} is obtained as follows:

$$(C_Q)(V_{CH}(x) - V(x)) - \beta|V_{CH}(x)|V_{CH}(x) + q(N_{Nitride}(x) - P_{Boron}(x)) = 0$$

$$\beta = \frac{q^3}{\pi(\hbar v_F)^2}. \tag{13}$$

Here, we assume that the first band has a dominant contribution to the charge transmission properties because other bands are completely distinct and separated from the conduction (valence) bands. Ballistic resistance of the electrodes per unit width then may be obtained from (15) [50]

$$R_{Electrode} = (\pi/2)(h/q^2)\sqrt{\hbar v_F/q|F_{Barrier}|} \tag{14}$$

where $F_{Barrier}$ is the electric field in the junction of p (n) doped region and barrier.

The simulation results for the capacitors of the four proposed structures within the NDR region ($V_{bias} = 0.65$ V) which are calculated by derivatives of the stored charges ($|\delta Q_{CH}/\delta V|$) versus RTD bias potential are presented in Table I [Fig. 5]. Also, device resistances are obtained from the equation $[-(\Delta V_{peak} - \Delta V_{valley})/(\Delta I_{peak} - \Delta I_{valley})]$.

Table I indicates that the "Rhombic Barrier" structure has a lower quantum capacitor value than the other three proposed structures. This smaller capacitor is due to the: 1) faster discharge of electrons between the two poles because of the dominant edge energy states in the charge transport and 2) minor electron trap in the ribbon due to the lack of a complete separator between the two poles.

From the circuit point of view, higher values of resistance can result in unstable operation. In this regard, the rhombic barrier structure has the best results. However, at the

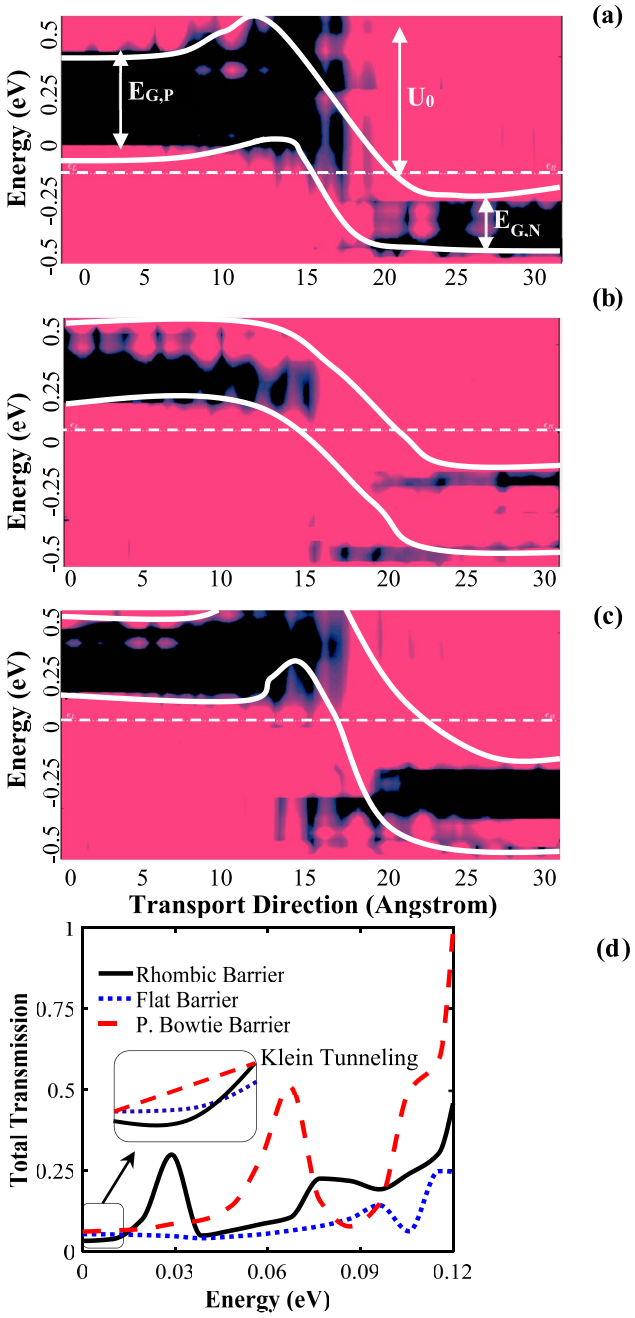

Fig. 6. (a)–(c) LDoS along with conduction and valence bands versus the structure length at 300 K. (d) Total transmission probability. This diagram is obtained by summing energy states of the LDoS (E, z, x) along with the length of the device [LDoSx (E, z)].

same time, this structure has more sensitivity to defect than other proposed devices due to its dominant edge energy states in the charge transport that shall be discussed further in the next section.

IV. Results

The local density of states (LDoS) of the proposed structures indicating the energy levels is shown in Fig. 6(a)–(c). Also, the total transmission spectrum is shown in Fig. 6(d). A total transmission peak depicts available energy levels in the charge transport direction. Furthermore, the existence of transmission probability near the Fermi level represents the Klein tunneling

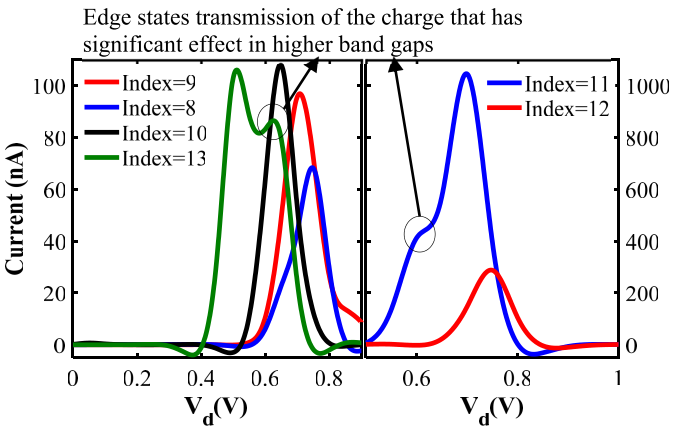

Fig. 7. Current–voltage curves of the flat barrier structure for different widths corresponding to 8–13 indexes. The same colors denote the same GNR class ($3n$, $3n+2$).

effect that is observable in Fig. 6. Klein tunneling is eliminated when U_0 is greater than the $E_{G,P(N)}$ that is in accordance with the previous studies [51]. However, more doping density results in an increased Klein tunneling probability. The summary of the values is reported in Table II.

Flat barrier structure I–V curves corresponding to the total transmission spectrum for different widths corresponding to 8–13 indices are shown in Fig. 7. As shown in Fig. 7, changing the device width, which usually has a severe effect on the GNR bandgap, slightly affects the maximum current bias position. Furthermore, the 3.5× enhancement of the peak current value due to the 3-Å width increase is obtained.

The structure index should be larger than a specific number in order to achieve high stable PVRs since the bandgap variations versus width are lower in wider GNRs. Based on the simulation results, the minimum recommended index is 13. Therefore, from hereafter, all the simulations are evaluated with this condition [Fig. 7].

From another point of view, Fig. 7 shows that the current originates from two sources (which results in two NDR curves): 1) the current due to the edge energy states and 2) the current generated by free inner energy states of the impurity atoms and the structural defects.

The edge energy states (the first source) are not useful because device characteristics show a high sensitivity to edge defects, which is described further. Therefore, this contribution must be eliminated, and then it is expected that the NDR bias position does not depend on the width of the structure. This idea, of course, results in decreasing the maximum current value which results in PVR degradation. To overcome this problem, the two Bowtie and Flat structures and also a combination of them can be used. Since the number of –C–B and C–N bonds is identical in the BN-edges structure, they make the same number of positive and negative charge carriers in the two sides of the device. This charge separation in the normal charge transport direction creates a transverse electric field. The transverse electric field with neutralization of the opposite charge carriers reduces electronic transport [29].

As the length of the structure increases, we expect that the peak current bias position does not change and it only affects the current values. The simulation results depict that increasing

TABLE II
ELECTRONIC PROPERTIES OF THE PROPOSED STRUCTURES VERSUS 8, 11, AND 13 INDEXES OF FLAT BARRIER AND INDEX OF 13 FOR THE OTHER ONES. HERE, POWER CONSUMPTION IS CALCULATED IN THE CURRENT VALLEY BIAS POINT

Type	Index	Max. Current Pos. (V)	Max. Current (nA)	Min. Current Pos. (V)	Min. Current (nA)	PVR	Power Consumption (nW)	C.P.
Flat	W=8	0.37	15.5	0.44	6.6	2.3	2.9	0.035
Flat	W=11	0.42	51.6	0.54	7	7.37	3.8	0.38
Flat	W=13	0.65	109.3	0.75	5.1×10^{-2}	2143	0.038	234
I.Bowtie	W=13	0.6	463	0.7	1.2	385	0.84	178
Rhombic	W=13	0.8	1256	0.9	364	3.45	328	4.3
P.Bowtie	W=13	0.65	450	0.75	0.1	4500	0.075	2025

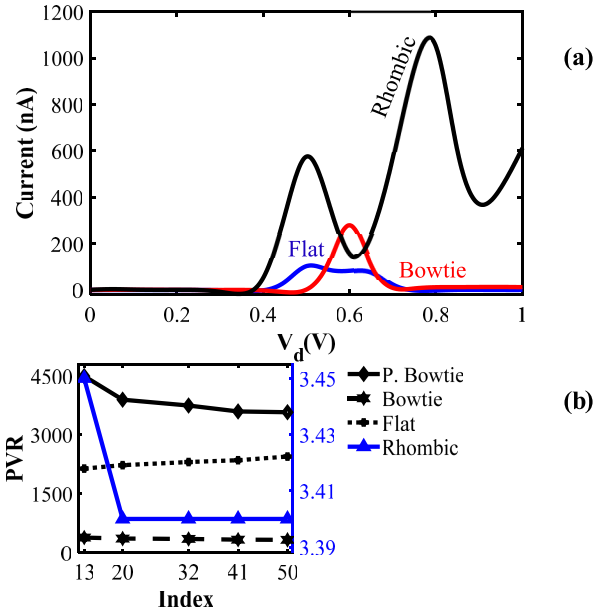

Fig. 8. (a) Current–voltage curves for the three proposed structures (index = 15). (b) PVR versus index for the proposed structures.

the length of the BN barrier region reduces the probability of tunneling of the electron-wave (6), which significantly reduces the valley current and also somewhat reduces the peak current.

In the last survey, Fig. 9 shows some of the device configurations that are considered to verify the robustness of the proposed devices to essential types of defects. However, edge vacancy defects are the most critical defects in the structures below 60-nm width [52]. In the reported results, such defects can cause severe degradation of performance of the devices, which generally eliminate the NDR in the I–V characteristic [15], [53]. This degradation mainly comes from potential fluctuation in the GNR bandgap.

Green's function trend of [54] is used. Also, tight binding onsite and hopping (bonding) parameters are used from [55]. The presence of such an off-plane displacement of atoms (resulting from the optimization process [56]) and defects affect the hopping integral elements. Assuming that the perturbative potential smoothly evolves on the range of one atomic orbital, [57] used a Hückel formulation using electrostatic summation method to describe the influence of these distortions on the nondiagonal Hamiltonian elements using electrostatic correction.

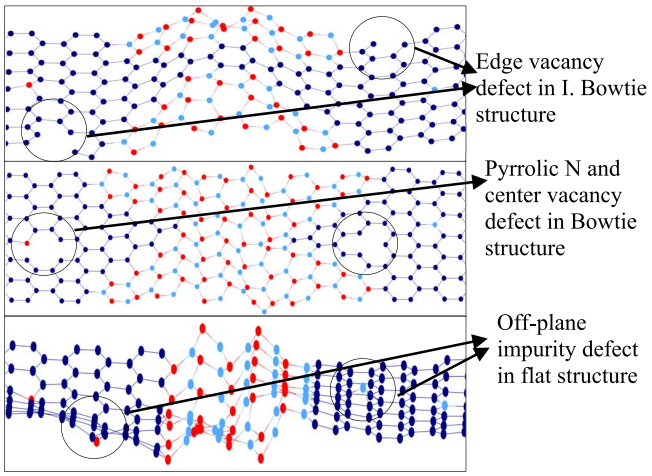

Fig. 9. Three different structural defects that were surveyed.

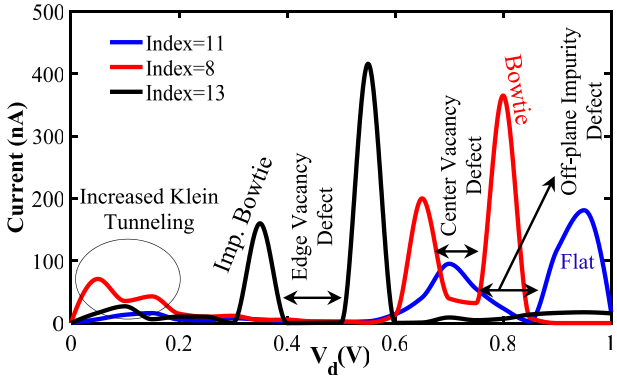

Fig. 10. I–V diagram with the presence of edge vacancy defects.

Applying the edge defects which are considered as the worst defects, only the maximum current degradation due to increased scattering is observed as shown in Fig. 10. Yet, NDR is observable. However, impurity introduces a random voltage fluctuation in the graphene layer, which causes a shift of the Dirac point and finally results in increased conductivity. At high carrier densities, such charged impurities act as scattering sources which reduce the mobility of the intrinsic graphene to a limited value [58]. As mentioned earlier, the impurity atoms result in reduced dependence of the charge transport on the edge energy states. Besides, Fig. 10 shows that all the defect types have two NDRs with some bias differences between them. This difference depends on the kind of defects.

TABLE III
EFFECTS OF DIFFERENT TYPES OF DEFECTS ON THE MIN/MAX CURRENT RATIO. NUMBERS ARE IN THE FORM OF $I_{WITH\ DEFECTS}/I_{WITHOUT\ DEFECTS}$ IN %

Defect Type	Barrier Region				Extended Electrode			
Inner Vacancy	86*	28	49	63.1	63	36	52	58.6
Edge Vacancy	15.3	69.4	8.2	38	6.5	75	9.4	45
Inner Impurity	51.4	65.9	11.2	27.6	67.3	59.1	71.3	21
Edge Impurity	69.5	32.7	17.9	36.9	58.6	41	14.8	21.6
	FLAT	**Im. Bowtie**	**Rhombic**	**Per. Bowtie**	**FLAT**	**Im. Bowtie**	**Rhombic**	**Per. Bowtie**

*This result is excellent but in practice it destroys the barrier region.

TABLE IV
SUMMARY OF SIMULATION RESULTS FOR THE FOUR PROPOSED STRUCTURE AND OTHER WORKS IN THE LITERATURE

Index	Max. Current Pos.(V)	Max. Current (nA)	Min. Current Pos. (V)	Min. Current (nA)	PVR	Power Consumption (pW)
FLAT Barrier[1]	0.65	109.3	0.75	5.1e-2	2143	38
Imperfect Bowtie Barrier[1]	0.6	463	0.7	1.2	385	840
Rhombic Barrier[1]	0.8	1256	0.9	364	3.45	3.28×10^{5}
Perfect Bowtie Barrier[1]	0.65	450	0.75	0.1	4500	75
[13] (Antidot-BN doping)	0.064	4.13	0.088	0.825	5	72.73
	0.064	0.02	0.088	7×10^{-4}	29.4	0.06
[14] (Strain induced)	0.083	56.25	0.133	14.97	3.75	-
[1] (GNR h-BN)	0.55	220	0.75	100	-	-
[15] (Step-like GNR)	0.35	20×10^{3}	0.6	15×10^{3}	1.3	9×10^{6}
[16] (H, W shape GNR)	0.07	4.9	0.1	9.8×10^{-3}	540	
[19] (new structure)	0.024	122	0.07	0.0143	8582	-
[60] (N doped GNR)	0.2	1×10^{3}	0.6	20	50	12×10^{3}

[1] The results are obtained using index=13

Furthermore, defects generally increase Klein tunneling. The results of applying two types of defects (vacancy and doping) in the inner or the edge of both p (n) doped and the barrier regions for the four proposed structures are summarized in Table III.

This comprehensive table is obtained by averaging the results of 350 simulation runs from the different geometries of defect positions. Also, Table IV provides a comparison between the results of the new proposed structures and other papers reported in the literature.

V. CONCLUSION

In this paper, a new bipolar structure that we have called RDSLD is proposed that includes Flat, Perfect and Imperfect Bowtie and Rhombic barrier shaped structures that have several outstanding features. Notably, the proposed structures are robust to a few types of defects (impurity and vacancy) and also have high values of PVR and CP. Furthermore, a comprehensive survey on the ac model and the effects of the geometrical parameters on the transmission probability of charged carriers is conducted.

In this paper, a PVR of about 400 has been reached with 3-nm ribbon length, which is far better than the traditional structures presented in the literature. Moreover, the results prove that the presence of defects does not eliminate the NDR property and only degrades the maximum current value. According to the results, the new device can be a basis for the development of practical devices based on graphene.

REFERENCES

[1] J. Gaskell *et al.*, "Graphene-hexagonal boron nitride resonant tunneling diodes as high-frequency oscillators," *Appl. Phys. Lett.*, vol. 107, no. 10, 2015, Art. no. 103105.

[2] H. Mizuta and T. Tanoue, *The Physics and Applications of Resonant Tunnelling Diodes; Cambridge Studies in Semiconductor Physics and Microelectronic Engineering 2*. Cambridge, U.K.: Cambridge Univ. Press, 1995.

[3] H. Yokoyama, H. Sugiyama, M. Asada, A. Teranishi, and S. Suzuki, "Fundamental oscillation of resonant tunneling diodes above 1 THz at room temperature," *Appl. Phys. Lett.*, vol. 97, no. 24, 2010, Art. no. 242102.

[4] A. C. Ferrari *et al.*, "Science and technology roadmap for graphene, related two-dimensional crystals, and hybrid systems," *Nanoscale*, vol. 7, no. 11, pp. 4598–4810, Sep. 2015.

[5] R. Ciriminna, N. Zhang, M. Q. Yang, F. Meneguzzo, Y. J. Xu, and M. Pagliaro, "Commercialization of graphene-based technologies: A critical insight," *Chem. Commun.*, vol. 51, no. 33, pp. 7090–7095, 2015.

[6] M. D. Stoller, S. Park, Y. Zhu, J. An, and R. Ruoff, "Graphene-based ultracapacitors," *Nano Lett.*, vol. 8, no. 10, pp. 3498–3502, Sep. 2008, doi: 10.1021/nl802558y.

[7] A. A. Balandin *et al.*, "Superior thermal conductivity of single-layer graphene," *Nano Lett.*, vol. 8, no. 3, pp. 902–907, 2008.

[8] C. Lee, X. Wei, J. W. Kysar, and J. Hone, "Measurement of the elastic properties and intrinsic strength of monolayer graphene," *Science*, vol. 321, no. 5887, pp. 385–388, 2008.

[9] R. Yadav and C. K. Dixit, "Synthesis, characterization and prospective applications of nitrogen-doped graphene: A short review," *J. Sci. Adv. Mater. Devices*, vol. 2, no. 2, pp. 141–149, Jul. 2017.

[10] W. Tian, W. Li, W. Yu, and X. Liu, "A review on lattice defects in graphene: Types, generation, effects and regulation," *Micromachines*, vol. 8, no. 5, p. 163, May 2017.

[11] G. N. Dash, S. R. Pattanaik, and S. Behera, "Graphene for electron devices: The panorama of a decade," *IEEE J. Electron Devices Soc.*, vol. 2, no. 5, pp. 77–104, Sep. 2014.

[12] D. K. Ferry, "The role of substrate for transport in graphene," in *Proc. IEEE Nanotechnol. Mater. Devices Conf.*, Oct. 2012, pp. 43–48.

[13] A. Y. Goharrizi, M. Zoghi, and M. Saremi, "Armchair graphene nanoribbon resonant tunneling diodes using antidote and BN doping," *IEEE Trans. Electron Devices*, vol. 63, no. 9, pp. 3761–3768, Sep. 2016.

[14] M. Zoghi and A. Y. Goharrizi, "Strain-induced armchair graphene nanoribbon resonant-tunneling diodes," *IEEE Trans. Electron Devices*, vol. 64, no. 10, pp. 4322–4326, Oct. 2017.

[15] Y. P. An *et al.*, "Negative differential resistance and rectification effects in step-like graphene nanoribbons," *Organic Electron.*, vol. 17, pp. 262–269, Feb. 2015.

[16] H. Teong, K.-T. Lam, and G. Liang, "A computational study on the device performance of graphene nanoribbon resonant tunneling diodes," *Jpn. J. Appl. Phys.*, vol. 48, Apr. 2009, Art. no. 04C156.

[17] H. Teong, K.-T. T. Lam, S. B. Khalid, and G. Liang, "Shape effects in graphene nanoribbon resonant tunneling diodes: A computational study," *J. Appl. Phys.*, vol. 105, no. 8, 2009, Art. no. 084317.

[18] H. Sevinçli, M. Topsakal, and S. Ciraci, "Superlattice structures of graphene-based armchair nanoribbons," *Phys. Rev. B, Condens. Matter*, vol. 78, no. 24, 2008, Art. no. 245402.

[19] M. Sharifi, E. Akhoundi, and H. Esmaili, "Negative differential resistance in new structures based on graphene nanoribbons," *J. Comput. Electron.*, vol. 15, no. 4, pp. 1361–1369, 2016.

[20] P. Palla, G. R. Uppu, A. S. Ethiraj, and J. P. Raina, "Bandgap engineered graphene and hexagonal boron nitride for resonant tunnelling diode," *Bull. Mater. Sci.*, vol. 39, no. 6, pp. 1441–1451, Oct. 2016.

[21] Y. Song, H.-C. Wu, and Y. Guo, "Negative differential resistances in graphene double barrier resonant tunneling diodes," *Appl. Phys. Lett.*, vol. 102, no. 9, 2013, Art. no. 093118.

[22] A. Mishchenko *et al.*, "Twist-controlled resonant tunnelling in graphene/boron nitride/graphene heterostructures," *Nature Nanotechnol.*, vol. 9, pp. 808–813, Oct. 2014.

[23] V. H. Nguyen, F. Mazzamuto, A. Bournel, and P. Dollfus, "Resonant tunnelling diodes based on graphene/h-BN heterostructure," *J. Phys. D. Appl. Phys.*, vol. 45, no. 32, pp. 17–19, Jul. 2012.

[24] N. Manavizadeh, F. Raissi, E. A. Soleimani, M. Pourfath, and S. Selberherr, "Performance assessment of nanoscale field-effect diodes," *IEEE Trans. Electron Devices*, vol. 58, no. 8, pp. 2378–2384, Aug. 2011.

[25] M. O. Li, D. Esseni, J. J. Nahas, D. Jena, and H. G. Xing, "Two-dimensional heterojunction interlayer tunneling field effect transistors (Thin-TFETs)," *IEEE J. Electron Devices Soc.*, vol. 3, no. 3, pp. 200–207, May 2015. [Online]. Available: http://ieeexplore.ieee.org/document/7006653/

[26] C. Zheng *et al.*, "Direct observation of 2D electrostatics and ohmic contacts in template-grown graphene/WS_2 heterostructures," *ACS Nano*, vol. 11, no. 3, pp. 2785–2793, Feb. 2017.

[27] L. Chen *et al.*, "Oriented graphene nanoribbons embedded in hexagonal boron nitride trenches," *Nat. Commun.*, vol. 8, Mar. 2017, Art. no. 14703.

[28] S. Bru *et al.*, "On-surface synthesis of BN-substituted heteroaromatic networks," *ACS Nano*, vol. 9, no. 9, pp. 9228–9235, Aug. 2015.

[29] A. Mehri, M. Jamaati, and A. Namiranian, "Electron transport in graphene/h-BN lateral hybrids: Rhombus and bowtie domains," *Superlattices Microstruct.*, vol. 109, pp. 264–272, Sep. 2017.

[30] G. H. Han *et al.*, "Continuous growth of hexagonal graphene and boron nitride in-plane heterostructures by atmospheric pressure chemical vapor deposition," *ACS Nano*, vol. 7, no. 11, pp. 10129–10138, Nov. 2013.

[31] Z. Liu *et al.*, "In-plane heterostructures of graphene and hexagonal boron nitride with controlled domain sizes," *Nat. Nanotechnol.*, vol. 8, no. 2, pp. 119–124, Jan. 2013.

[32] G. Bepete, D. Voiry, M. Chhowalla, Z. Chiguvare, and N. J. Coville, "Incorporation of small BN domains in graphene during CVD using methane, boric acid and nitrogen gas," *Nanoscale*, vol. 5, no. 14, pp. 6552–6557, 2013.

[33] L. Tapasztó, G. Dobrik, P. Lambin, and L. P. Biró, "Tailoring the atomic structure of graphene nanoribbons by scanning tunnelling microscope lithography," *Nat. Nanotechnol.*, vol. 3, no. 7, pp. 397–401, Jun. 2008.

[34] X. Li, X. Wang, L. Zhang, S. Lee, and H. Dai, "Chemically derived, ultrasmooth graphene nanoribbon semiconductors," *Science*, vol. 319, no. 5867, pp. 1229–1232, 2008.

[35] A. Seitsonen *et al.*, "Atomically precise bottom-up fabrication of graphene nanoribbons," *Nature*, vol. 466, no. 7305, pp. 470–473, Jul. 2010.

[36] X. Wang *et al.*, "N-doping of graphene through electrothermal reactions with ammonia," *Science*, vol. 324, no. 5928, pp. 768–771, May 2009.

[37] S. Mammadov *et al.*, "Work function of graphene multilayers on SiC(0001)," *2D Materials*, vol. 4, no. 1, 2017, Art. no. 015043.

[38] H. Ilatikhameneh, T. Ameen, F. Chen, H. Sahasrabudhe, G. Klimeck, and R. Rahman, "Dramatic impact of dimensionality on the electrostatics of P-N junctions and its sensing and switching applications," *IEEE Trans. Nanotechnol.*, vol. 17, no. 2, pp. 293–298, Mar. 2018.

[39] P. Rani and V. K. Jindal, "Designing band gap of graphene by B and N dopant atoms," *RSC Adv.*, vol. 3, no. 3, pp. 802–812, 2013.

[40] J. H. Chen, C. Jang, S. Adam, M. S. Fuhrer, E. D. Williams, and M. Ishigami, "Charged-impurity scattering in graphene," *Nat. Phys.*, vol. 4, no. 5, pp. 377–381, Apr. 2008.

[41] S. Adam, E. H. Hwang, V. M. Galitski, and S. Das Sarma, "A self-consistent theory for graphene transport," *Proc. Nat. Acad. Sci. USA*, vol. 104, no. 47, pp. 18392–18397, 2007.

[42] V. M. Galitski, S. Adam, and S. D. Sarma, "Statistics of random voltage fluctuations and the low-density residual conductivity of graphene," *Phys. Rev. B, Condens. Matter*, vol. 76, no. 24, Dec. 2007, Art. no. 245405.

[43] G. C. Solomon, C. Herrmann, T. Hansen, V. Mujica, and M. A. Ratner, "Exploring local currents in molecular junctions," *Nature Chem.*, vol. 2, pp. 223–228, Feb. 2010, doi: 10.1038/NCHEM.546.

[44] S. Datta, *Quantum Transport: Atom to Transistor*. Cambridge, U.K.: Cambridge Univ. Press, 2005.

[45] M. S. Fahad, A. Srivastava, A. K. Sharma, and C. Mayberry, "Analytical current transport modeling of graphene nanoribbon tunnel field-effect transistors for digital circuit design," *IEEE Trans. Nanotechnol.*, vol. 15, no. 1, pp. 39–50, Nov. 2016.

[46] H. Ilatikhameneh, R. B. Salazar, G. Klimeck, R. Rahman, and J. Appenzeller, "From fowler-nordheim to nonequilibrium Green's function modeling of tunneling," *IEEE Trans. Electron Devices*, vol. 63, no. 7, pp. 2871–2878, Jul. 2016.

[47] H. Lu, D. Esseni, and A. Seabaugh, "Universal analytic model for tunnel FET circuit simulation," *Solid-State Electron.*, vol. 108, pp. 110–117, Jun. 2015.

[48] A. Y. Goharrizi, M. Pourfath, M. Fathipour, H. Kosina, and S. Selberherr, "An analytical model for line-edge roughness limited mobility of graphene nanoribbons," *IEEE Trans. Electron Devices*, vol. 58, no. 11, pp. 3725–3735, Nov. 2011.

[49] S. Frégonèse, M. Magallo, C. Maneux, H. Happy, and T. Zimmer, "Scalable electrical compact modeling for graphene FET transistors," *IEEE Trans. Nanotechnol.*, vol. 12, no. 4, pp. 539–546, Jul. 2013.

[50] L. M. Zhang and M. M. Fogler, "Nonlinear screening and ballistic transport in a graphene *p-n* junction," *Phys. Rev. Lett.*, vol. 100, no. 11, Mar. 2008, Art. no. 116804.

[51] V. H. Nguyen, A. Bournel, and P. Dollfus, "Resonant tunneling structures based on epitaxial graphene on SiC," *Semicond. Sci. Technol.*, vol. 26, no. 12, pp. 1–7, Nov. 2011.

[52] Y. Yang and R. Murali, "Impact of size effect on graphene nanoribbon transport," *IEEE Electron Device Lett.*, vol. 31, no. 3, pp. 237–239, Mar. 2010.

[53] Y. An and Z. Yang, "Abnormal electronic transport and negative differential resistance of graphene nanoribbons with defects," *Appl. Phys. Lett.*, vol. 99, no. 19, Oct. 2011, Art. no. 192102.

[54] M. Noei, M. Fathipour, and M. Pourfath, "A computational study on the electronic properties of armchair graphene nanoribbons confined by boron nitride," *Jpn. J. Appl. Phys.*, vol. 51, no. 3, pp. 1–6, Mar. 2012.

[55] G. Seol and J. Guo, "Bandgap opening in boron nitride confined armchair graphene nanoribbon," *Appl. Phys. Lett.*, vol. 98, no. 14, pp. 2011–2014, Apr. 2011.

[56] J. H. Los, J. M. H. Kroes, K. Albe, R. M. Gordillo, M. I. Katsnelson, and A. Fasolino, "Extended Tersoff potential for boron nitride: Energetics and elastic properties of pristine and defective h -BN," *Phys. Rev. B, Condens. Matter*, vol. 96, no. 18, p. 184108, 2017.

[57] R. Zoubkoff, F. Triozon, Y. M. Niquet, and S. Latil, "Boron and nitrogen codoping effect on transport properties of carbon nanotubes," *Phys. Rev. B, Condens. Matter*, vol. 90, no. 12, 2014, Art. no. 125418.

[58] J. Xia, *Charge Transport and Quantum Capacitance of Graphene*. Tempe, AZ, USA: Arizona State University, 2010.

[59] H. Ren, Q. X. Li, Y. Luo, and J. Yang, "Graphene nanoribbon as a negative differential resistance device," *Appl. Phys. Lett.*, vol. 94, no. 17, 2009, Art. no. 1731103.